# A Data-Driven Optimization Framework for Industrial Demand-Side Flexibility

Carlo Manna[a], Manu Lahariya[b], Farzaneh Karami[c,d], Chris Develder[b]

[a]*Flemish Institute Technological Research (VITO), Belgium*
[b]*IDLab – imec, Ghent University, Ghent University, 26656 Gent, 9052, Belgium*
[c]*Ghent University, Dept. of Electromechanical, Systems and Metal Engineering, EEDT-DC, Flanders Make, Gent, 9052, Belgium*
[d]*KU Leuven, Dept. of Computer Science, CODeS, Gebroeders De Smetstraat 1, 9000, Gent, Belgium*

**Abstract**

Securing profits while offering industrial demand-side flexibility in both energy and reserve markets is critical to ensure the profitability of energy-intensive industrial plants to make available their flexible assets in the electricity markets and hence accelerating the energy transition. Proposing efficient bidding strategies for simultaneous participation in the energy and reserve market is challenging since it requires the integration of different market mechanisms in a single optimization problem (combining energy and reserve markets), as well as an accurate mathematical model of industrial processes from which to obtain energy flexibility. Often, such mathematical models are either not available or are described through complex simulators, making the design of a computationally efficient bidding strategy a complicated task.

This paper introduces a novel framework to support energy-intensive industrial plants to offer energy flexibility in the joint energy and reserve market. We use a neural network to model the complex nonlinear dynamics of the industrial flexible process. Then, to reduce the complexity of the resulting optimization process we convert the neural network into linear constraints, formulating the problem of bidding energy flexibility into the electricity market as a mixed-integer linear program. The uncertainties of the process variables are considered using a scenario-based approach.

A realistic simulation considering the case of an evaporative cooling tower used in the chemical industry, participating in the Belgian electricity market is carried out to demonstrate the applicability of the proposed scheme.

*Keywords:* Electricity markets, Industrial demand response, Energy flexibility, Neural networks, Mixed-integer-linear programming

## 1. Introduction

### *1.1. Motivation*

Sustainable development requires transition in energy consumption habits and human activities [19]. A shift from the use of fossil and non-renewable resources to the exploitation of renewable ones is now considered as crucial to preserve the future environment and meet sustainable development goals. To accomplish these objectives, the global energy system must undergo a profound transformation, by enhancing energy efficiency and investing in renewable energy solutions. In this context, the idea of energy flexibility or Demand-Side Flexibility (DSF) has become a common concept to encourage the integration of renewable energy sources (RES) into the power systems, and hence to accelerate the energy transition [16, 33]. Energy flexibility refers to the ability of a generic prosumer to change their energy consumption patterns based on external signals . It relates to the ability to address short-run and unexpected imbalances between demand and supply due to the increasing penetration of RES.

For this reason, DSF is now seen as an essential feature to turn the current energy-inefficient system into one dominated by renewable energy. New flexibility may come from various sources that will have to be exploited over the next years, e.g., through new storage technologies, increased sectorial coupling, industrial demand-side flexibility management], or improvements in operational efficiency through technological development [26, 39]. Industrial processes/plants are extensive energy consumers and play a key role in the reduction of energy demand and in developing advanced strategies based on energy flexibility [37].

**Nomenclature**

**Abbreviations**

| | |
|---|---|
| *DA* | Day Ahead |
| *TSO* | Transmission System Operator |
| *DSO* | Distribution System Operator |
| *DSF* | Demand-side Flexibility |
| *ECT* | Evaporative Cooling Tower |
| *IA* | Interval Arithmetic |

**Indices, sets and functions**

| | |
|---|---|
| $t$ | index of time, $t \in \mathcal{T}$ |
| $k$ | index for scenario, $k \in \mathcal{K}$ |
| $n$ | index for neurons in neural network, $n \in \mathcal{N}$ |
| $m$ | index for neural network layer input, $m \in \mathcal{M}$ |
| $l$ | index for neural network layer, $l \in \mathcal{L}$ |
| $o$ | index for order block, $o \in \mathcal{O}$ |
| $\mathcal{F}_n(\cdot)$ | nonlinear function |

**Parameters**

| | |
|---|---|
| $\Delta t$ | Time discretization step [s] |
| $\hat{T}^{out}$ | Estimated outdoor temperature [Celsius] |
| $\hat{H}$ | Estimated relative humidity [%] |
| $\hat{Q}^{p}$ | Estimated heat load (production process) [kJ] |
| $\hat{Q}^{t}$ | Estimated heat load (heat process) [kJ] |
| $\hat{A}$ | Estimated atmospheric pressure [Pa] |
| $\hat{U}^{c}$, $\hat{D}^{c}$ | Estimated upward and downward sequence of activation calls (binary) |
| $\Omega^{c}$, $\Omega^{c}$ | Uncertainty budget denoting maximum numbers of upward and downward activation calls |
| $\rho$ | Battery loss coefficient |
| $\eta_c$, $\eta_d$ | Battery charging and discharging efficiency |
| $C$ | Provider fixed cost in using flexibility [€] |
| $\hat{\lambda}$ | DA energy market price [€/MWh] |
| $\hat{\lambda}^{u}$, $\hat{\lambda}^{d}$ | Upward and downward market prices [€/MWh] |
| $\hat{\lambda}^{+}$, $\hat{\lambda}^{-}$ | Surplus and deficit unbalancing cost [€/MWh] |
| $\underline{P}$, $\overline{P}$ | Maximum and minimum power for the cooling fan [kW] |
| $\underline{P}^{E}$, $\overline{P}^{E}$ | Maximum and minimum charging/discharging power for the battery [kW] |
| $\underline{E}$, $\overline{E}$ | Maximum and minimum energy capacity for the battery [kWh] |
| $\underline{T}$, $\overline{T}$ | Maximum and minimum temperature for the water basin [°C] |

**Decision variables**

| | |
|---|---|
| $p$ | Electrical power [kW] |
| $p^{\mathrm{D}}$ | Total electrical power to buy/sell in the DA energy market [kW] |
| $p^{\mathrm{F}}$ | Fan cooling controlling power for the planned working cycle. Contribution to the total power $p^{\mathrm{D}}$ [kW] |
| $p^{\mathrm{BC}}$, $p^{\mathrm{DC}}$ | Battery charging and discharging power for the planned working cycle. Contribution to the total power $p^{\mathrm{D}}$ [kW] |
| $c^{\mathrm{UP}}$, $c^{\mathrm{DW}}$ | Upward and downward capacity reservation [kW] |
| $p^{\mathrm{ch}}$, $p^{\mathrm{dh}}$ | Battery charging and discharging powers [kW] |

**Auxiliary variables**

| | |
|---|---|
| $T^{\mathrm{b}}$ | Water basin temperature [°C] |
| $p^{\mathrm{au}}$, $p^{\mathrm{ad}}$ | Activation upward and downward powers [kW] |
| $p^{\mathrm{s+}}$, $p^{\mathrm{s-}}$ | Surplus and deficit electrical powers [kW] |
| $E$ | State-of-charge for the battery [kWh] |
| $\alpha$ | neuron activation (binary) |

In a liberalized market environment, the actual flexibility dispatch is largely driven by the offering strategy of the entity who owns and operates these flexible assets. A private investor/operator aims at maximizing its expected profit. Typical revenue streams originate from price arbitrage in day-ahead wholesale energy markets and the provision of ancillary services such as operating reserves. In this regard, efficient offering strategies often require the simultaneous preparation (co-optimization) of bids in multiple markets in order to improve the economic value of flexibility assets as shown in many studies [10, 25, 42, 51];

For this reason, the aim of this paper is to propose a novel optimization framework to enable bidding energy flexibility of industrial processes in the both energy and reserve market.

In order to design such a bidding strategy, it is necessary to develop models with the capability of predicting the effect of control settings on the systems' dynamic behavior. However, modelling industrial processes and their components is very challenging, and often the traditional models and parameters describing the process dynamics to be controlled are not available in practice [22, 5].

Unlike analytical models, data-driven approaches [15], such as neural networks, are very accurate and do not require the knowledge/availability of the mathematical equations and internal parameters of the process to be controlled [44, 36, 8]. However, using nonlinear data-driven models in complex optimization problems either implies the use of nonlinear iterative solution methods (which are often computationally expensive) or heuristic search (that do not guarantee high-quality solutions [21]).

To overcome the aforementioned computational issues, in this paper, we first use a neural network to accurately model the (energy-flexible) industrial process and then, through an exact linear transformation, we encode such a neural network in a number of linear constraints, formulating the problem of bidding flexibility in the joint energy and reserve market as Mixed-Integer Linear Programming (MILP). In this way, the resulting optimization problem can be solved efficiently using standard mathematical solvers such as: Gurobi, Cplex, etc. Finally, we further reduce the complexity of the initial formulation using various techniques, including ReLU pruning for weight matrix sparsification and interval arithmetic [46].

As a case study, to demonstrate the applicability of the proposed approach, we focus on evaporative cooling towers (ECT) as part of the chemical process industry and one of the major energy demand drivers in the industrial sector [3]. In particular, we simulated an ECT participating in the joint energy and reserve Belgian market for 24 hours. We used simulated data for the ECT process variables and real data for the weather and the electricity market prices. We first analyze the performances for two case studies in which the flexibility of the ECT is augmented by coupling it with electrical storage and then evaluate the computational aspects.

### *1.2. Related work*

A vast portion of the recent literature in the context of proposing bidding strategies for industrial settings focus on the use of electrical energy storage.

Despite the fact that electrical energy storage is difficult to model accurately due to a number of factors including uncertainty parameters, state-of-charge estimation and performance decay, most of the recent approaches assume energy storage as either linear or simplified nonlinear models with uncertainty parameters and propose bidding strategies using various linear optimization techniques [14].

On the other side, another portion of literature, instead of considering electrical storage as the only flexible asset of an industrial process, focuses on considering the industrial process itself (or some of its components) as a source of energy flexibility. Such a distinction adds to the problem a further degree of complexity due to the process modeling and the impact from assuming flexible operations on the process variables.

In this regard, different approaches have been proposed for industrial evaporative cooling tower (ECT) management systems aiming to improve energy efficiency and reduce carbon emissions [35]. ECT system is a (energy-intensive) thermal utility process, where thermal inertia is linked to the core process, which allows it to be controlled in a flexible manner.

In general, for ECT systems, two types of approaches are found in the literature. The first type of methods are simulation-based models for the assessment and prediction of key performance indicators such as costs, energy and water demand. They are addressed in particular either with mathematical optimization methods [11] or scenario-based simulation [32, 41]. Such methodologies use complex mathematical models or simulators to describe the physical process for the ECT system and its components. A second type of techniques are mainly operational methods for specific activities (e.g. monitoring of water temperatures, quality, reduction of down-times by optimizing maintenance activities, etc.) based on short-time forecasts and black-box approaches to model the ECT systems [18, 28, 43, 45].

However, none of the above methods are developed to exploit the energy flexibility of the ECT industrial process into the electricity market. Consequently, the proposed optimization strategies do not consider the market mechanism and their operational constraints or other random variables such as market prices, reserve activation calls, etc.

In this regard, several studies have proposed different strategies to exploit industrial process energy flexibility into the electricity market. The authors in [34] propose a synergetic approach of data-driven and scenario-based simulation to evaluate different demand-side strategies to improve the overall energy efficiency, while the work

in [24] report a case study for Denmark's electricity market, where various ECT management strategies have been applied in order to offer energy flexibility in different markets (e.g.: day-ahead, reserve provision etc.). However, such aforementioned strategies were predefined and not optimally planned through optimization techniques.

Conversely, optimization-based approaches can be found in [2] where a mixed-integer programming model is proposed for a hybrid flow shop schedule with preventive maintenance actions, to minimize energy cost for an enterprise under the time-of-use tariff scheme. Moreover, the work in [4] proposes a data-driven method to integrate energy flexibility in production planning, while in [47] the flexibility of a cryogenic energy storage is exploited in order to perform load shifting. Both methods aim to reduce the plant running cost by storing purchased energy and selling it back to the market during higher-price periods and creating additional revenue by providing operating reserve capacity.

On the same line, the works in [7, 9, 38, 48, 49, 50] for aluminum smelters and steel plants, which analyze the opportunity to participate in the day-ahead energy and reserve market to reduce the overall production costs. All these approaches are based both on the use of simulation models of the process to investigate the opportunity to participate in the energy market [7, 9, 38], and on proper bidding strategies through MILP formulation and the use of approximate linear models of the process [48, 49, 50].

Although the aforementioned methods can be considered as bidding strategies, they are aimed at participating in individual markets, while, as mentioned in the §1.1, an efficient way to maximize the market profits is to develop bidding strategies for simultaneous participation in multiple markets.

On this line of research, the authors in [17] developed a bidding strategy for the joint day-ahead and reserve market for a pulp and paper mill, based on a two-stage stochastic programming approach. Nonetheless, they use a linear simplified model to represent the pulp/paper mill plants, due to the lack of a more accurate mathematical model and process-dependent parameters.

### *1.3. Research gaps and main contributions*

In the body of literature surveyed, we found two main research gaps:

1. the first gap is that the reported bidding strategies are limited to participation in single markets, while there is a lack of methods that explore the opportunity to participate in multiple markets (e.g. day-ahead, reserve market, etc.) at the same time (co-optimization);

2. the mathematical models used to describe the process to be controlled and used in the bidding strategies are mainly approximate analytical models or simulators. However, such models assume the knowledge of process parameters that are hardly available in practice [3, 35]. Conversely, a little has been done in the field literature to propose optimal bidding methods that make use of data-driven approaches to describe the process model.

.

Regarding point 1, one of the main contributions of this paper is to propose an innovative data-driven optimization framework to support the valorization of the energy flexibility of an industrial cooling tower system in the joint energy and reserve market. This is particularly complex, as it is necessary to consider, simultaneously, different market mechanisms, which in turn lead to different operational constraints deriving from market-specific implementation rules and different forms of uncertainties. As such, we have considered the uncertainty of process load (i.e., the thermal energy required to run the specific industrial operations), market prices, reserve activation requests from the Transmission System Operator (TSO) and other contextual exogenous variables (i.e.: outdoor temperature, humidity and atmospheric pressure) which are incorporated using a set of scenarios generated from available day-ahead forecasts.

Then, regarding the point 2, in this paper we use black-box methods (i.e. deep neural networks) to model the nonlinear industrial cooling tower process, and use this model in an optimal bidding strategy through a Mixed-Integer Linear Programming (MILP) formulation. This is not a straightforward task, as using nonlinear black-box models in optimization problems implies the use of Local Search, meta-heuristics, or Genetic Algorithms [21], which often do not guarantee high quality solutions. For this reason, we first develop a neural network to model the ECT process using realistic data and then, through an exact transformation we convert it into a set of linear constraints with binary variables, encoding a deep (nonlinear) neural network transition model into a MILP model. In this way, we accurately approximate cost-optimal solutions of the original nonlinear optimization problem that can be solved through a standard mathematical solver (e.g., Gurobi, CPLEX, etc.).

In summary, the main contributions of this paper are:

- A data-driven stochastic optimization model to address the participation of power-intensive industrial processes in the energy and reserve markets;
- A mixed-integer linear formulation of the original black-box optimization problem, using a neural network to model the energy-intensive process. Such a formulation guarantees cost-optimal solutions and the computational tractability of the problem.

Moreover, we remark that the proposed approach can be generalized to other industrial demand-side applications where a computationally tractable mathematical model of the process involved is not available, while it is possible to describe such a system dynamic using a neural-networks in a sufficiently accurate manner.

The remainder of this paper is organized as follows: Section 2 discusses the proposed methodology in detail, numerical experiments are described in the Section 3 and results are reported in the Section 4. Finally the conclusions are summarized in the Section 5.

## 2. Proposed methodology

### *2.1. Demand-side flexibility in the electricity market*

In the energy sector, DSF refers to the possibility of adjusting the electrical consumption or the electrical production of an installation or process in response to an external signal, as for instance a price signal, an activation signal from the grid operator for dispatching balancing reserves, etc. Therefore, DSF can be implemented and exploited in different ways depending on the type of electricity market and grid service in which it is delivered.

As mentioned in §1.3, this paper focus on two type of markets: the energy and the tertiary reserve market.

In the **energy market**, DSF means taking advantage of *price fluctuations* on the energy exchanges. This allows shifting energy consumption to moments with lower prices, and energy production (or injection of energy surplus) to moments with higher prices. On the other hand, in the **reserve market**, DSF is delivered by either lowering or increasing the power consumption (denoted as upward and downward reserve activation respectively) up to a specific (pre-contracted) amount to balancing the power grid following a signal sent by the grid operator which then compensates providers for the provision of these balancing services.

Offering flexibility in the aforementioned markets means submitting bids that consist of both energy quantities (in the energy market) and upward/downward power capacity quantities (in the reserve market) which are remunerated at certain market prices to the flexibility provider. In both cases, those bids are the result of optimal strategies which calculate the offered quantities taking into account market price estimates and operational/technological constraints of the providers.

### *2.2. Assumptions on Market Structure*

The industrial facility participates in the DA energy market with bids to buy and sell energy. Furthermore, it sells manual reserve in the tertiary reserve market (in both upward and downward directions). The tertiary (or non-spinning) reserve is a service manually activated by the transmission system operator (TSO) to handle forecast errors and/or to replace the secondary reserve. The DA energy market is a double-sided auction, where market agents may present sell and buy hourly bids that cover the 24 hours of the next day and are paid at a marginal price.

Downward and upward tertiary reserve bids are presented to the TSO until a specific hour (may be different from country to country) of the day prior to the operating day, and they can be updated during the operating day. The reserve bids comprise a quantity (MW) and an hourly price (Eur/MWh) and they are dispatched by an economic merit order in real-time. The downward and upward reserves are remunerated by the respective marginal prices. There are two possible market-clearing schemes. A sequential market where energy is traded first and reserves are contracted afterward (typically European). A joint market where energy and reserves are jointly dispatched (typically American). The approach described in this paper can be applied to both market schemes. In particular, in this paper, we refer to the Belgium electricity market, where the most simple form of daily bids consists of 24 offers of 1-hour block each.

All the participants are assumed as price-takers, as the exchanged volume of energy by each individual participant is not so large as to influence the market price. Each participant has access to time series of past market prices and exchanged quantities of energy and capacity reserves which they can use to analyze and predict the next day's market prices.

In the following section, the proposed approach for simultaneous participation in the energy and tertiary reserve market for a DSF provider with an industrial evaporative cooling tower process is detailed.

### *2.3. Bidding Optimization Strategies for the ECT flexibility valorization in electricity markets*

In this section, two mathematical models to bid ECT flexibility in the joint energy and reserve market are for-

mulated and solved.

The first model considers the ECT system as the only flexible asset, while the second one combines the ECT with another flexible asset, i.e. an electrical storage system.

For sake of clarity, we name the first approach as *cooling tower flexibility strategy* (in short **C-Flex**), and the second one as *cooling tower with storage flexibility strategy* in short **CWS-Flex**.

### *2.3.1. C-Flex mathematical model*

The objective function along with the constraints are given below:

$$\max \overbrace{\sum_t p_t^{\mathrm{D}}(\hat{\lambda}_t - \mathrm{C}_t)\,\Delta t}^{\text{expected profit (energy m.)}} + \overbrace{\sum_t \left[c_t^{\mathrm{UP}}\hat{\lambda}_t^{\mathrm{u}} + c_t^{\mathrm{DW}}\hat{\lambda}_t^{\mathrm{d}}\right]}^{\text{expected profit (reserve m.)}}$$
$$\overbrace{+\frac{1}{K}\sum_{k,t}\left[\, p_{k,t}^{\mathrm{au}}(\hat{\lambda_t^{\mathrm{au}}} - \mathrm{C}_t) + \; p_{k,t}^{\mathrm{ad}}(\hat{\lambda_t^{\mathrm{ad}}} - \mathrm{C}_t)\right]}^{\text{expected profit from reserve activation}} \tag{1}$$
$$\overbrace{-\frac{1}{K}\sum_{k,t}\left[\, p_{k,t}^{\mathrm{s+}}\;\hat{\lambda}_t^{+} + p_{k,t}^{\mathrm{s-}}\;\hat{\lambda}_t^{-}\right]}^{\text{expected penalty}}$$

**s.t.**:

$$p_{k,t}^{\mathrm{au}} = c_t^{\mathrm{UP}}\hat{U}_{k,t}^{\mathrm{call}} \tag{2}$$
$$p_{k,t}^{\mathrm{ad}} = c_t^{\mathrm{DW}}\hat{D}_{k,t}^{\mathrm{call}} \tag{3}$$
$$\underline{P}_t \le p_{k,t} \le \overline{P}_t \tag{4}$$
$$T_{k,t+1}^{\mathrm{b}} = \mathcal{F}_n(T_{k,t}^{\mathrm{b}}, \hat{Q}_{k,t}^{\mathrm{p}}, \hat{Q}_{k,t}^{\mathrm{b}}\hat{T}_{k,t}^{\mathrm{out}}, \hat{H}_{k,t}, \hat{A}_{k,t}, p_{k,t}) \tag{5}$$
$$\underline{T}_t \le T_{k,t}^{b} \le \overline{T}_t \tag{6}$$
$$\underline{T}_{\mathrm{init}} \le T_{k,t}^{\mathrm{b}} \le \overline{T}_{\mathrm{init}} \tag{7}$$
$$\underline{T}_{\mathrm{end}} \le T_{k,t}^{\mathrm{b}} \le \overline{T}_{\mathrm{end}} \tag{8}$$
$$p_{k,t} = p_t^{\mathrm{D}} + p_{k,t}^{\mathrm{ad}} - p_{k,t}^{\mathrm{au}} + p_{k,t}^{\mathrm{s+}} - p_{k,t}^{\mathrm{s-}} \tag{9}$$
$$(p_{k,t}^{\mathrm{s+}}, p_{k,t}^{\mathrm{s-}}) \ge 0 \tag{10}$$
$$(c_t^{\mathrm{UP}}, c_t^{\mathrm{DW}}) \ge 0 \tag{11}$$

The objective function (1) has four main terms. The first term in line 1 (left side) describes the expected profits gained from the energy market, expressed as the offered energy quantities $p_t^D$ at the predicted market prices $\hat{\lambda}_t$. The quantity $C_t$ denotes a generic fixed operational cost for the flexibility provider. On the other hand, the second term in line 1 (right side) represents the expected profit from the reserve market formulated as the product of the offered capacity reservations $c_t^{UP}$ (upward) and $c_t^{DW}$ (downward), multiplied the estimated remuneration prices $\hat{\lambda}_t^u$ and $\hat{\lambda}_t^d$, respectively.

The third term (line 2) represents the expected profit from the upward and downward reserve activation calls at the operating stage. This is expressed as the average sum of the upward ($p_{k,t}^{au}$) and downward ($p_{k,t}^{ad}$) capacity activation multiplied the corresponding estimated remuneration prices $\hat{\lambda}_t^{au}$ and $\hat{\lambda}_t^{ad}$, over the total number of scenarios $K$.

Finally, the last term (line 3) reports the expected penalty incurred in case there is any surplus or deficit of power with respect to the quantity committed in the DA market (both energy and reserve), over the total number of scenarios $K$. In particular, $p_{k,t}^{s+}$ ($p_{k,t}^{s-}$) denotes the surplus (shortfall) of power supplied during the operational stage following an activation call, in relation to the amounts contracted in the DA stage (line 1). Such deviations (surplus or deficit) will be penalized according to the estimated penalty prices $\hat{\lambda}_t^+$ and $\hat{\lambda}_t^-$, respectively

The uncertainty of calling the capacity of reserve market from the TSO is modeled by implementing a budget of uncertainty for the maximum number of reserve calls for each scenario. In particular, in this formulation, two uncertainty budgets are introduced, i.e., $\Omega_k^{\mathrm{U}}$ and $\Omega_k^{\mathrm{D}}$, indicating the maximum number of intervals that up and down reserves are called from the TSO, respectively. For example, if we set $\Omega_k^{\mathrm{U}} = 4$, we are assuming that a maximum of 4 timesteps of up reserve calls occur from the TSO for scenario $k$ with $k = 1 \dots K$.

The auxiliary parameters $\hat{U}_{k,t}^{\mathrm{call}}$ and $\hat{D}_{k,t}^{\mathrm{call}}$ with their related subscripts define the estimated time intervals that the facility is called for up and down reserve respectively, holding the relation $\sum_t \hat{U}_{k,t}^{\mathrm{call}} = \Omega_k^{\mathrm{U}}$ ($\sum_t \hat{D}_{k,t}^{\mathrm{call}} = \Omega_k^{\mathrm{D}}$ ), where $\Omega_k^U$ denotes the total number of reserve activation calls for the scenario $k$. Hence, if $\hat{U}_{2,3}^{\mathrm{call}} = 1$, this mean that at timestep 2 of the scenario 3, the upward reserve must be deployed.

Constraints (2-3) determine the power for upward and downward activation respectively taking into account the quantities $\hat{U}_{k,t}^{\mathrm{call}}$ and $\hat{D}_{k,t}^{\mathrm{call}}$. In particular, they state that these activated quantities are always equal to the full committed capacity $c_t^{\mathrm{UP}}$ or $c_t^{\mathrm{DW}}$. Notice that it must hold $\hat{U}_{k,t}^{\mathrm{c}} + \hat{D}_{k,t}^{\mathrm{c}} \le 1$ for each $t = 1 \dots T$ and $k = 1 \dots K$. This implies that an upward and a downward activation call cannot occur at the same time step.

Constraint (9) defines the controlled power input as a contribution of three elements: (*i*) the power requested in the DA market $p_t^{\mathrm{D}}$, (*ii*) the power from the down-

ward or upward activation $p^{\text{ad}}_{k,t}$ or $p^{\text{au}}_{k,t}$, respectively, and (*iii*) an additional power $p^{\text{s+}}_{k,t}$ or $p^{\text{s-}}_{k,t}$. Such an additional power component represents, respectively, a surplus or a deficit in electrical power with which to scale the quantity $p_{k,t}$ whether necessary for the purpose of complying with other technological constraints. These constraints are the maximum and minimum controlling power (4), the boundaries of the basin temperature (6) and its initial and final conditions (7) and (8), respectively. Then, constraints (10) and (11) state, respectively, that the surplus/deficit power components and the upward/downward capacity reservations must be non-negative quantities.

Finally, the eq. (5) represents the mathematical model of the ECT system which describes the temporal evolution of the water basin temperature $T^{b}_{k,t+1}$.

This is a nonlinear model represented through a neural network. In particular, at each time step $t$ and for each scenario $k$, this model receives as input the estimation of the outdoor temperature $\hat{T}^{\text{out}}_{k,t}$, the humidity $\hat{H}_{k,t}$ and the atmospheric pressure $\hat{A}_{k,t}$, along with the estimated heat load for the production process $\hat{Q}_{k,t}$. The other inputs are the water basin temperature $T^{b}_{k,t}$ and the control variable $p_{k,t}$ (i.e. electrical power of the cooling fans).

### *2.3.2. CWS-Flex mathematical model*

This mathematical model differs from the previous one by adding additional constraints that take into account the combined use of the ECT system with an electrical storage. Hence, the objective function remains the relation (1), while the related constraints are reported below:

$$\text{eqs.}(2) - (8)$$

$$p^{\text{D}}_{t} = p^{\text{F}}_{t} + p^{\text{BC}}_{t} - p^{\text{BD}}_{t} \tag{12}$$

$$p_{k,t} = p^{\text{F}}_{t} + p^{\text{ad}}_{k,t} - p^{\text{au}}_{k,t} + p^{\text{dh}}_{k,t} - p^{\text{ch}}_{k,t} + p^{\text{s+}}_{k,t} - p^{\text{s-}}_{k,t} \tag{13}$$

$$E_{k,t+1} = \rho E_{k,t} + \left[\eta_{\text{c}}\ (p^{\text{ch}}_{k,t} + p^{\text{BC}}_{t})\ - \eta_{\text{d}}\ (p^{\text{dh}}_{k,t} + p^{\text{BD}}_{t})\right]\ \Delta t \tag{14}$$

$$\underline{P}^{\text{E}} \leq (p^{\text{ch}}_{k,t} + p^{\text{BC}}_{t}) \leq \overline{P}^{\text{E}} \tag{15}$$

$$\underline{P}^{\text{E}} \leq (p^{\text{dh}}_{k,t} + p^{\text{BD}}_{t}) \leq \overline{P}^{\text{E}} \tag{16}$$

$$\underline{E} \leq E_{k,t} \leq \overline{E} \tag{17}$$

$$\underline{E}_{\text{init}} \leq E_{k,t} \leq \overline{E}_{\text{init}} \tag{18}$$

$$\underline{E}_{\text{end}} \leq E_{k,t} \leq \overline{E}_{\text{end}} \tag{19}$$

$$(p^{\text{s+}}_{k,t}, p^{\text{s-}}_{k,t}, p^{\text{ch}}_{k,t}, p^{\text{dh}}_{k,t}) \geq 0 \tag{20}$$

$$(c^{\text{UP}}_{t}, c^{\text{DW}}_{t}, p^{\text{BC}}_{t}, p^{\text{BD}}_{t}) \geq 0 \tag{21}$$

where the set of constraints (2)-(8) are identical to the set of constraints in the section 2.3.1.

The condition (12) states that the electrical power from the DAM is the sum of the planned electrical power for the cooling fan $p^{\text{F}}_{t}$ and either the planned charging or discharging power (i.e., $p^{\text{BC}}_{t}$ or $p^{\text{BD}}_{t}$) for the electrical storage. These *planned* quantities are scenario independent and they concern the electrical powers accounted for the DAM offers.

Equation (13) defines the electrical power fan $p_{k,t}$ for the scenario $k$ as the sum of the planned power for the cooling fan $p^{\text{F}}_{t}$, plus other scenario-dependent quantities such as the power from either the downward or upward activation (i.e., $p^{\text{ad}}_{k,t}$ or $p^{\text{au}}_{k,t}$, respectively); the power to compensate either a surplus ($p^{\text{s+}}_{k,t}$) or a deficit ($p^{\text{s-}}_{k,t}$) in the total electrical load to satisfy any other system constraints and, finally the power to either charge ($p^{\text{ch}}_{k,t}$) or discharge ($p^{\text{dh}}_{k,t}$) the electrical storage. Equation (14) tracks the evolution of the state-of-charge for the battery system, while constraints (15)-(16) define the minimum and maximum charging and discharging battery power. Then, (17) defines the battery capacity, while constraints (18-19) set the related initial and final conditions for the state-of-charge. Finally, (20) and (21) define the non-negative variables in the model.

## *2.4. MILP encoding using neural network*

In this section we explain the procedure we used to reformulate the neural networks in (5) as linear constraints and hence, to convert both optimization problems reported in the §2.3.1 and §2.3.2 to an equivalent MILP.

First, we describe the fundamental approach to reformulation, and then we describe additional methods to reduce the complexity of the fitted neural network in order to improve solver performance.

### *2.4.1. Reformulation of ReLU as linear constraints*

Let $n$ be the number of neurons, $l$ the number of layers and $m$ the number of inputs for that layer. Moreover, let $x^{l-1}_{k,t,n,m}$ denoting the $m$-th input at the neuron $n$ of the layer $l$.

In a neural network, the inputs for each layer are first combined as:

$$y^{l}_{k,t,n} = a_{n,0} + \sum_{m} a^{l-1}_{n,m}\ x^{l-1}_{k,t,n,m} \tag{22}$$

where $a_{n,m}$ are the coefficients of the weight matrix $(n, m+1)$ of the layer $l$.

The output of the linear combination (22) becomes the input of the chosen activation function. In this approach, since we use ReLU activation function, the final output of the neuron $n$ at the layer $l$ is:

$$y_{k,t,n} = \max(0,\ y^l_{k,t,n}) \tag{23}$$

Equation (22) represents a linear relation between the inputs and outputs for each layer $l$, therefore it can be encoded inside the optimization models in the § 2.3.1 and § 2.3.2 without any problems as linear equality constraint.

Conversely, (23) is a non-linearity that needs to be reformulated, using the following set of constraints:

$$y_{k,t,n} \geq y^l_{k,t,n} \tag{24}$$

$$y_{k,t,n} \leq L^{\max}\ \alpha_{k,t,n} \tag{25}$$

$$y_{k,t,n} \geq 0 \tag{26}$$

$$y_{k,t,n} \leq y^l_{k,t,n} - L^{\min}\ (1 - \alpha_{k,t,n}) \tag{27}$$

$$\alpha_{k,t,n} \in \{0,\ 1\} \tag{28}$$

where the value for the parameters $L^{\max}$ and $L^{\min}$ need to be chosen large enough to guarantee the respect of the ReLU activation function (23). Such a method is described in the next section.

We introduce one binary variable for each neuron in the hidden layers of the neural network. In case the input to the neuron is $y^l \leq 0$, then the corresponding binary variable is 0 and (25) and (26) constrain the neuron output $y$ to 0. Conversely, if the input to the neuron is $y^l \geq 0$, then the binary variable is 1 and (24) and (27) constrain the neuron output $y$ to the input $y^l$.

Once we have defined the neural network using (22) and (24) - (28), we replace those conditions in (5), obtaining a MILP formulation for the optimization models in § 2.3.1 and § 2.3.2.

#### *2.4.2. Weights matrix sparsification*

As aforementioned in the § 2.4.1, the minimum and maximum bounds on each neuron output $L^{\min}$ and $L^{\max}$ have to be chosen large enough to bind the conditions (24)-(28), but also as small as possible to facilitate tight bounds and hence improve the computational efficiency of the MILP solver.

For this reason, we compute these bounds using interval arithmetic (IA) [30]. In IA, the bounds on each neuron are determined solely by considering the bounds on the variables in the previous layer.

Moreover, we adapt the idea of ReLU pruning [46] in this context, to prune away ReLU functions that are not necessary and hence reduce the total number of binary variables. In particular, first we calculate the bounds $L^{\min}_n$ and $L^{\max}_n$ for each neuron using IA. Then, we select, for each pair ($L^{\min}_n$,$L^{\max}_n$) associated with neuron $n$, those that have the limits ($L^{\min}_n$,$L^{\max}_n$) both positive or both not positive (i.e. $\leq 0$). In the first case, this means that such ReLU will be always active. That is, according with (23), it holds that $y_{k,t,n} = y^l_{k,t,n}$ for any input $y^l_{k,t,n}$. Conversely, in the second case, the ReLU will be always inactive, i.e. $y_{k,t,n} = 0$ for any input $y^l_{k,t,n}$. Finally, if a ReLU is always active, it will be replaced with an identity function, while in the other case with a null function. In both cases, we reduce the total number of ReLU activation functions and therefore the need to introduce a binary variable as described in (24)-(28).

## 3. Experimental details

### *3.1. Simulation Setup*

As a test case, we considered an ECT owner who participates in the energy and tertiary reserve market during 2017. To simulate realistic data, we use the white-box model outlined in previous literature [20]. This thermodynamic-based white-box model of the cooling tower system is represented by a system of first-order differential equations that are based on the laws of heat transfer and mass conservation. This model is presented in (29) where $T^b_{k,t}$ denotes the basin temperature. This model is defined using $Q^p_{k,t}$ the process heat $[W]$, $Q^t_{k,t}$ the cooling capacity $[W]$, $c_w$ the specific heat capacity of water $[kJ/kg \cdot K]$, $V_w$ the water volume $[m3]$ and $\rho_w$ the water density $[kg/m3]$.

$$\frac{\partial T^b_{k,t}}{\partial t} = \frac{Q^p_{k,t} - Q^t_{k,t}}{c_w \cdot V_w \cdot \rho_w} \tag{29}$$

$$Q^p_{k,t} = \dot{m}_w \cdot c_w \cdot (T^p_{k,t} - T^b_{k,t}) \tag{30}$$

$$Q^t_{k,t} = \dot{m}_a \cdot (H^{a,e}_{k,t} - H^{a,l}_{k,t}) \tag{31}$$

The process heat ($Q^p_{k,t}$) is expressed as in (30) where $\dot{m}_a$ denotes the mass flow of water [Kg/s]. $T^p_{k,t}$ and $T^b_{k,t}$ are the process water temperature $[K]$ and the water basin temperature $[K]$, respectively. Note that the $\dot{m}_a$ is based on an individual industry, each with a different mass flow of its process water. The process heat ($Q^t_{k,t}$) is expressed as in (31). $\dot{m}_a$ is the mass flow of air $[Kg/s]$, $H^{a,e}_{k,t}$ and $H^{a,l}_{k,t}$ are the entering and leaving air enthalpy $[kJ/kg \cdot K]$, respectively. Enthalpies can be calculated using humidity rates and temperature [40]. The entering

air enthalpy is dependent on the temperature of the ambient air, and the leaving air enthalpy is dependent on the leaving air temperature. The mass flow rate of air depends on the power that is supplied to the fans and is expressed in (32). This will affect the basin temperature.

$$\dot{m}_a = \sqrt{\frac{2 \cdot P_f \cdot \rho_a \cdot A_{fr}^2 \cdot \eta_{fan} \cdot \eta_{motor}}{6.5 + K_{el} + 2 \cdot \frac{A_{fr}^2}{A_{fan}^2}}} \tag{32}$$

where $P_f$ is the electric fan power $[W]$, $A_{fr}$ is the tower frontal area $[m2]$, $A_{fan}$ is the fan area $[m2]$, $\eta_{fan}$ is the fan efficiency %, $\eta_{motor}$ is the motor efficiency % and $K_{el}$ is the eliminator coefficient and if it is unknown, it is set equal to 1. The air density is represented by $\rho_a$ and is calculated for the mixture of dry air and water evaporation.

We can estimate the basin temperate, $T^b_{k,t}$, based on the fan powers, process heat, and environmental data. For the cooling process, data is simulated for each minute from Jan $1^{st}$ 2017 to $31^{st}$ Dec 2017, i.e. 60 minutes $\times$ 24 hours $\times$ 365 days = $525,600$ observations. Thus, the duration of each timeslot is 1 minute and we create $1,440$ time slots for each day of 24 hours. Each day starts from midnight (00:00) and ends 24 hours later (23:59) and we represent each timeslot as a decimal value $\in [0.00, 24.00)$ (for example, a time slot with the value equal to 1.5 means 01:30 AM). A timeslot of 1 minute is chosen because: $(i)$ it provides sufficient training data compared to larger timeslots (e.g. 15 min), and $(ii)$ time-varying dependencies of the dynamic system are better captured compared to smaller time slots (e.g. 1s).

To simulate data, we select the power supplied to the fan for specified time intervals, representing the final value of power at the end of this interval. This power value is chosen randomly from a uniform distribution in the range $[100, 200)$. Fan power is linearly increased from the initial value (at the start of this selected interval) to the final value (at the end of the selected interval). For every interval, process heat is randomly sampled from a Gaussian distribution with a mean of 30 W and a standard deviation of 1 W. Gaussian noise is added to the simulated $T^b_{k,t}$ to get realistic training data for neural networks. Weather data (ambient temperature, pressure, and humidity) is collected for 2017 and used for calculating $Q^t_{k,t}$ [1].

The python package 'simpy' is used for simulation. The temperature range is assumed to be $9°C$. The operational limits of $T^b_{k,t}$ are assumed to be from $\underline{T}^t_{k,t} = 9°C$ to $\overline{T}^t_{k,t} = 36°$C, and the average efficiency is set to $1/\eta = 0.6$. A total of 5 datasets were simulated using the same weather data for 2017, thus resulting in data of 5 years.

### *3.2. Simulation design*

The numerical simulations reported in this section aim to show the applicability of the proposed models *C-Flex* and *CWS-Flex* described in the § 2.3.1 and § 2.3.2 respectively, by analyzing the related results in terms of expected profits. generation of bids and computational aspects. For this reason, a realistic experimental setting is investigated.

Simulations were carried out gradually increasing the number of scenarios considered, from 10 up to a maximum of 50. Then, the maximum number of scenarios were set to 50 since this was a trade-off between computation time and negligible fluctuation in the quality of the solutions.

In order to fit the ECT model with a neural network we split the dataset in 90% training and 10% test set and train a neural network with 3 hidden layers with 30, 50 and 20 neurons respectively. We used ReLU activation functions and applied interval arithmetic and ReLU pruning method as reported in § 2.4.2 to reduce the overall complexity of the resulting MILP formulation.

Finally, we obtain a trained neural network with a predictive accuracy of 99.5% on the test dataset, showing good generalization capability of the neural network.

We have considered the participant bidding simultaneously in the energy and the reserve market for three different days, i.e. February 15th, June 15th and October 15th of the 2017. We used the energy and reserve market prices for that days from the Belgian System Operator website [13].

Real datasets, for weather conditions and ECT-thermal load, were collected within the INDUFLEX/MOONSHOT project [23] and used to produce predictions.

In particular, we generated 50 different scenario profiles for the weather conditions and ECT-thermal load using the Gaussian Copula method [27]. For each of the aforementioned variables, we built a predictor using historical data. Then, the forecasts from such a predictors were used as explanatory variables for a quantile regression. We considered each scenario having the same probability of occurrence. The details of the scenario generation procedure are reported in appendix to this paper.

In this regard, we point out that probabilistic scenario generation is a vast research topic and finding accurate

scenario generation methodologies is out of the scope of this work.

To determine the upward and downward sequence of activation calls $\hat{U}^{\text{call}}_{k,t}$ and $\hat{D}^{\text{call}}_{k,t}$ respectively, for each of the 50 generated scenario we first have set the maximum number of activations $\Omega^{\text{U}}_k$ and $\Omega^{\text{D}}_k$. Then, for each scenario, the sequences $\hat{U}^{\text{call}}_{k,t}$ and $\hat{D}^{\text{call}}_{k,t}$ were generated randomly, keeping into account such a maximum number of activations.

We have set both $\Omega^{\text{U}}_k$ and $\Omega^{\text{D}}_k$ to 4 per day (i.e. 1 hours per day). This choice was inspired by a standard reserve activation scheme adopted by the Belgian System Operator [12].

In each scenario, the starting water basin temperature is randomly chosen in the interval [10°C, 20°$C$]. The same interval is considered for the minimum and maximum final temperature $\underline{T}_{\text{end}}$ and $\overline{T}_{\text{end}}$.

We assumed the maximum battery capacity $\overline{E}$ = 200 kWh and the minimum $\underline{E}$ = 0 kWh. Also, we set $\underline{E}_{\text{init}} = \underline{E}_{\text{end}} = 0.2\overline{E}$ and $\overline{E}_{\text{init}} = \overline{E}_{\text{end}} = 0.8\overline{E}$ for every scenario.

Finally, the efficiency charging $\eta_c$ and discharging $\eta_d$ are both set at 0.97 while we assumed the loss factor $\rho = 0.99$.

We used python programming language and PyTorch libraries to perform the training of the neural network.

The computational experiments were executed on a standard Dell Laptop, with Windows 10 Enterprise 64-bit operating system, an Intel(R) core(TM) *i*5 processors and 8GB of RAM.

The MILP formulation is solved using Gurobi 9.5.

## 4. Results

Figure 1 shows, for each of the 3 case studies analyzed (i.e., 3 different days of the year), the energy offers in the day-ahead market provided by the two proposed models: the model which includes the energy storage (i.e.: *CWS-Flex*) and the model without energy storage (i.e.: *C-Flex*).

In each of these case studies, the difference between the *C-flex* and *CWS-flex* models mainly consists in the fact that the latter generally tends to purchase energy (therefore with a negative profit) when the market price is lower, while it injects energy into the power network (with a positive profit) in the times of the day when the energy cost is higher. This behavior is evident in all cases showed in the figures 1a, 1b and 1c. As a result of the reported case studies, the daily expected cost for purchasing the energy necessary to run the ECT process is higher in the *C-Flex* model than in the *CWS-flex*

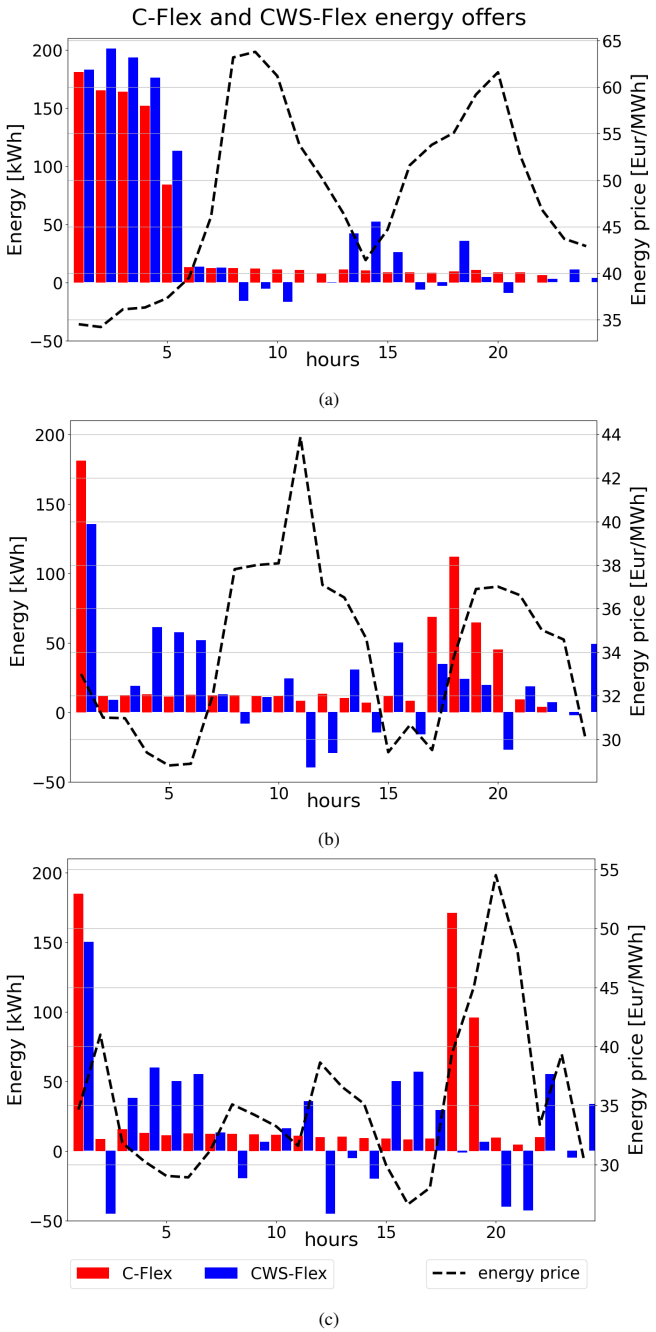


Figure 1: Energy offers and energy prices for (*a*) the 15th of February, (*b*) the 15th of June and (*c*) the 15th of October 2017 for both *C-Flex* and *CWS-Flex* model cases respectively.

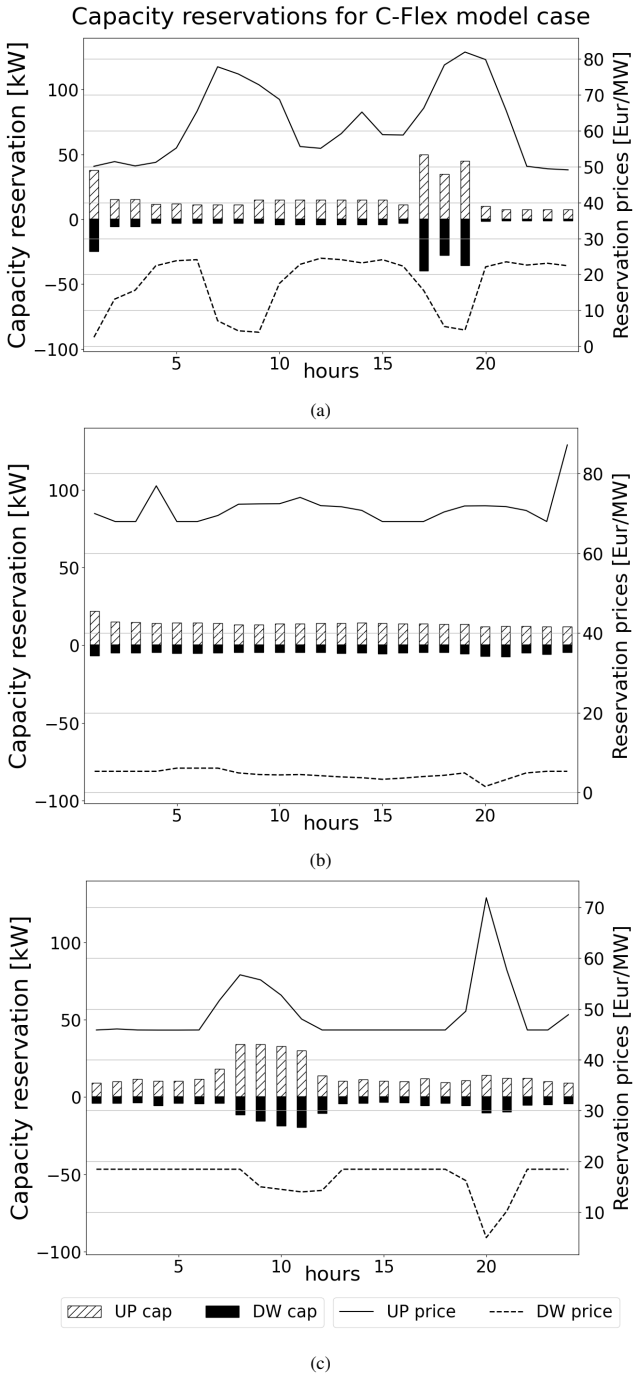


Figure 2: Upward and downward capacity reservations and prices for (*a*) the 15th of February, (*b*) the 15th of June and (*c*) the 15th of October 2017 for the *C-Flex* case.

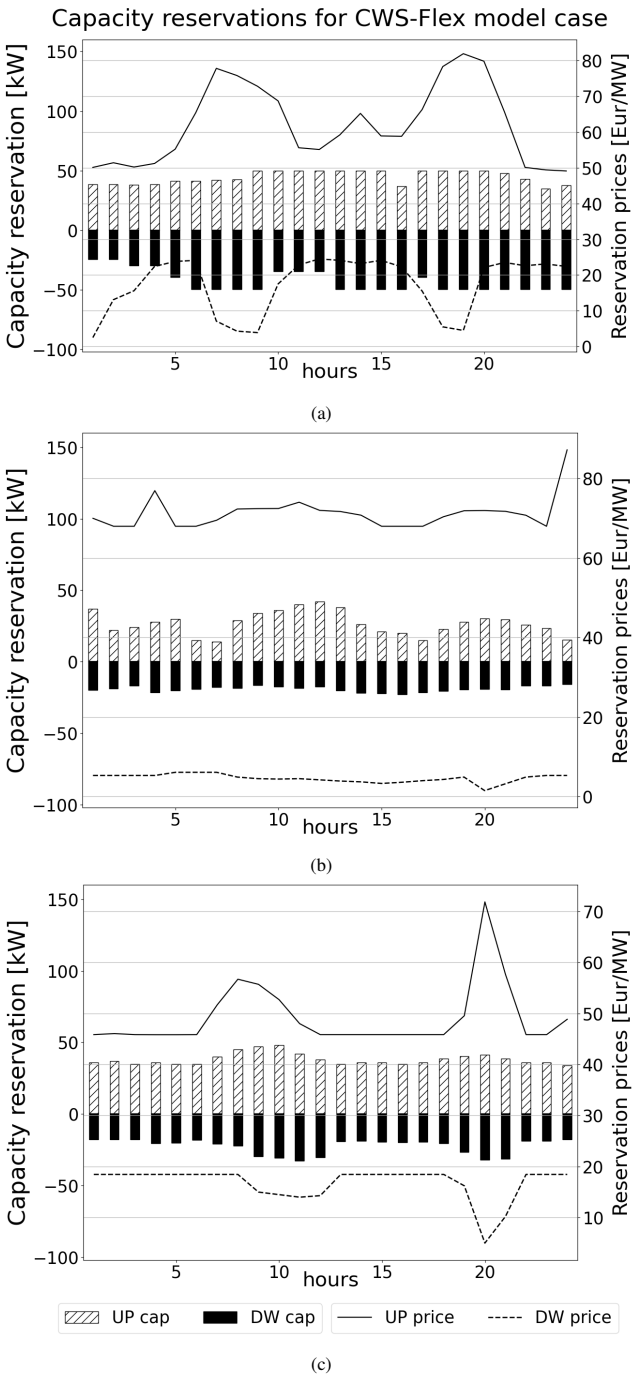


Figure 3: Upward and downward capacity reservations and prices for (*a*) the 15th of February, (*b*) the 15th of June and (*c*) the 15th of October 2017 for the *CWS-Flex* case.

model as shown in table 1 (i.e. in the first column: *energy* market type). This is because the battery included in such a model is used to store energy when it is economically more convenient to buy from the electricity market, and then use it to feed the ECT process while injecting any surplus into the electricity grid, reducing the daily net energy cost.

On the other hand, figures 2 and 3 show, in each of the case studies, the upward and the downward capacity reservations for the *C-Flex* and for the *CWS-Flex* model respectively.

Similarly to what resulting from the energy market, also in the reserve market, the *CWS-Flex* model produces higher capacity reservation quantities than the ones resulting from the *C-Flex* model in both upward and downward market for all the reported cases.

Particularly, the table 1 shows a comparison between the expected profit of the two proposed models both in the upward and in the downward market for the different simulated days of the year.

According to the table 1, considering the expected profit from the combined participation in the downward and upward markets, the use of an electrical storage in the *CWS-Flex* model results in increasing the expected profit by a factor ranging from a minimum of 0.86 to a maximum of 2.5 compared to the C-flex model without electrical storage.

In particular, the battery allows part of its capacity to be reserved in the event of an activation request from the grid operator, and therefore the available reserve capacity can generally be greater than what is available in the *C-Flex* case. In fact, the latter (without an electrical storage), can only decrease (downward) or increase (upward) its absorbed power within the limit allowed by the operational constraints of the CT process described in the 2.3.1, while the *CWS-Flex* model can store/inject an excess/reduction of power from or to the power grid using the battery. This concept is showed as illustrative example in the following paragraph.

### *4.1. Impact of the electrical storage on the capacity reservation*

Figures 4-6 show the electrical variables for the *CWS-Flex* model (i.e. $p_{k,t}$, $E_{k,t}$, $p^{s+}_{k,j}$ and $p^{au}_{k,t}$) and for the *C-Flex* model (i.e. $p_{k,t}$, $p^{s+}_{k,j}$ and $p^{au}_{k,t}$) respectively, in one typical scenario during the day of 15th of February.

For this scenario, the upward reservation capacity is around 50kW in both cases. However, in the *CWS-Flex* model (Fig. 4), the upward activation call $p^{au}_{k,t}$ (which requires lowering the total power absorbed from the grid of the same amount) is partially balanced by the discharging power $p^{dh}_{k,t}$ (for an amount of nearly 20kW) as

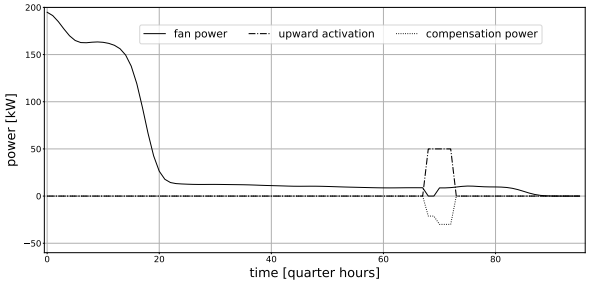


Figure 4: *CWS-Flex* model case: fan power ($p_{k,t}$), activation power ($p^{au}_{k,t}$) and compensation power ($p^{s+}_{k,j}$) profiles for a single scenario.

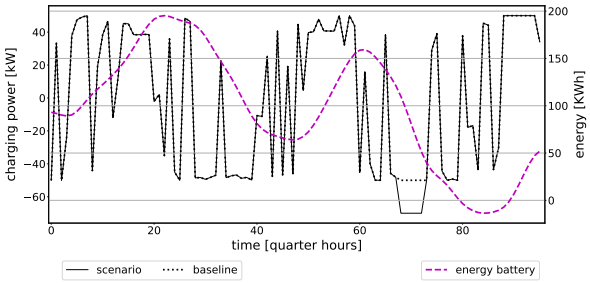


Figure 5: *CWS-Flex* model case: $p^{BC}_t/p^{DC}_t$ powers for the baseline charging and discharging cycle are reported with black dotted line, while the charging and discharging powers $p^{ch}_{k,t}/p^{dh}_{k,t}$ for the reported scenario $k$ are denoted with the continuous line. Dashed magenta line reports the energy battery $E_{k,t}$. Notice that the two charging/discharging cycles (i.e.: scenario and baseline) are exactly the same except at 17 : 00pm when the there is an additional discharging contribution from $p^{dh}_{k,t}$ of about 20kW to compensate the upward activation call $p^{au}_{k,t}$.

shown in Fig. 5. The rest of the upward activation call is covered by reducing the fan power $p_{k,t}$ and by the compensation power $p^{s+}_{k,j}$ for a value lower than 20kW (Fig. 4).

Conversely, in the *C-Flex* model (Fig. 6), the upward activation call $p^{au}_{k,t}$ is balanced almost entirely by the compensation power $p^{s+}_{k,j}$ and only partially by reducing the fan power $p_{k,t}$.

Since the compensation power is greater in the *C-Flex* model case than in the *CWS-Flex* case, this determines an increase of the penalty terms in eq. 1 which lower the profit expectation for the *C-Flex* model case compared to the *CWS-Flex* case.

### *4.2. Computational aspects*

Computational aspects are shown in Table 2, in which model statistics are organized by different number of total scenarios used for the proposed MILP models.

In such a table we also report the number of binary variables without applying the weight matrix sparsifica-

| market type | energy [€] | | upward res. [€] | | down. res. [€] | | TOTAL [€] | |
|---|---|---|---|---|---|---|---|---|
| | C | CWS | C | CWS | C | CWS | C | CWS |
| 15th February | −37.01 | −36.48 | 26.55 | 47.19 | 2.35 | 18.21 | **−8.12** | **28.92** |
| 15th June | −22.05 | −14.18 | 29.18 | 53.39 | 0.61 | 2.13 | **7.73** | **41.34** |
| 15th October | −24.34 | −10.75 | 12.69 | 45.54 | 2.82 | 8.91 | **−8.83** | **43.60** |

Table 1: Expected profit breakdown for both *C-Flex* and *CWS-Flex* model in the three analyzed case studies. The table shows the contribution of each market to the total profit reported in the eq. (1). Notice that the upward and downward reservation profits take into account the last 3 terms of the eq. (1), i.e. expected profit from: reserve market, reserve activation and expected penalty.

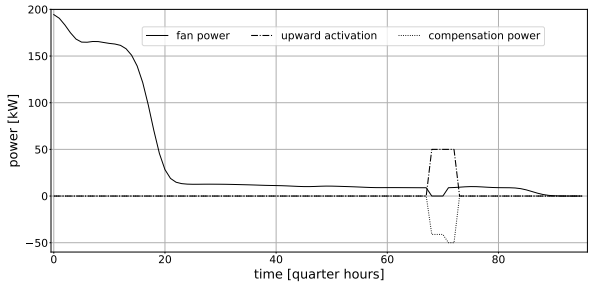


Figure 6: *C-Flex* model case: fan power ($p_{k,t}$), activation power ($p^{\text{au}}_{k,t}$) and compensation power ($p^{\text{s+}}_{k,j}$) profiles for a single scenario.

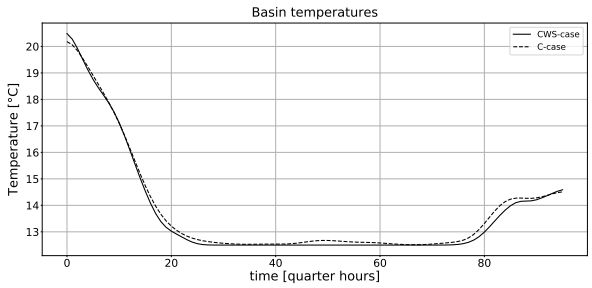


Figure 7: Water basin temperature profiles for *C-Flex* and *CWS-Flex* models. The temperature profiles shown correspond to the scenario considered through Figs. 4–6.

tion (i.e.: second row of the table 2) and the final number of binary variables for a reduced problem after using the methodologies detailed in the § 2.4.2 (i.e.: third row of the table 2).

Using matrix sparsification we were able to reduce the total number of binary variables of around 15-20 % (depending upon the number of considered scenarios). This facilitates the MILP solver computation time and increase the scalability.

As shown in table 2, even for the case of 50 scenarios, we achieve an average computation time of 7503 seconds (less than 2 hours) with a relative optimality gap of 0.0026 %.

## 5. Conclusions and Future Outlook

In this paper, we introduce a framework to bid energy flexibility of industrial process in the joint energy and reserve market. First, we use a deep neural networks with ReLU activation functions to capture the complexity and the non-linearity of the industrial process. Then, we convert the non-linear ReLUs into linear constraints using binary variables and formulate the bidding problem as a Mixed-Integer-Linear-Programming.

Finally we implement weight sparsity to reduce the complexity of the MILP problem to facilitate the MILP-solver execution.

Using realistic dataset, we demonstrate the applicability of the proposed framework considering an evaporative cooling tower used in the chemical industry and offering energy flexibility in the Belgian electricity market.

A first challenge of the proposed method consists in assuming Deep Neural Networks with only ReLU (or ReLU-like) activation functions. Although this may be a limitation, a vast literature in deep learning indicates such activation function having strong advantages over traditional activation functions (e.g., sigmoid and tanh), in reducing vanishing gradient issues, computational efficiency, and increasing convergence performance [15]. Moreover, the adoption of ReLU activations allows us to introduce binary decision conditions which are conceptually identical to the ones used in Decision-Tree based methods [6]. Therefore, the proposed framework could, in principle, be applied also to the case in which we use such approaches as approximating function instead of neural networks.

Furthermore, the proposed method considers a scenario-based uncertainty both for the parameters related to industrial process (outside temperature, heating demand, etc ) and for electricity market (market prices) . However, the quantification of the number of scenarios to be considered typically faces a trade-off between accuracy and computational efficiency. As such, in some use cases, the decision of the most suitable number of scenarios can be a complex task. This

| n. scenarios | 10 | 20 | 30 | 40 | 50 |
|---|---|---|---|---|---|
| Cont. variables | 203,924 | 407,464 | 611,004 | 814,544 | 1018,084 |
| Binary variables (original problem) | 96,000 | 192,000 | 288,000 | 384,000 | 480,000 |
| Binary variables (reduced problem) | 80,862 | 161,466 | 242,390 | 323,567 | 403,382 |
| Relative gap [%] | 0.000 | 0.000 | 0.0013 | 0.0018 | 0.0031 |
| Execution time [s] | 337 | 1199 | 2645 | 4280 | 7322 |

Table 2: Model statistics using different number of total scenario $K$ (average values).

challenge provides further research opportunities to expand on the current work. Indeed, to address these critical aspects in future research, different methodologies than the scenario-based approach can be considered (such as robust optimization or chance-constrained optimization)[31], evaluating them in terms of applicability and computational feasibility.

Finally, the proposed approach is based on a pure-data driven method. Despite it is technically possible to acquire and store huge amount of real-data, in many practical situations, the volume of useful experimental data for complex physical systems (e.g. industrial processes) is limited due to many factors (e.g. the cost of a pervasive sensor infrastructures, data-sharing privacy issues etc.) The specific data-driven approach to the predictive modelling of such systems depends crucially on the amount of data available and on the complexity of the system itself. For this reason, future work is directed towards utilizing different types of neural networks for modelling industrial processes, such as Physics-Informed Neural Networks [29]. These hybrid data-driven methods can be applied when the underlying physics of the process is partially known and several scattered measurements (of a primary or auxiliary state) are available. Integrating known (approximate) information about the underlying physics of the process to control, accurate data-driven models (such as neural networks) can still be constructed using much less amount of data compared with those necessary for pure data-driven methods.

## 6. Acknowledgment

Part of the research leading to these results has received funding from Agentschap Innoveren & Ondernemen (VLAIO) as part of the Strategic Basic Research (SBO) program under the InduFlexControl-1 project).

## Appendix: Scenario generation

Let $\hat{q}_{t+k}$ be a set of forecasted quantiles for the variable of interest $p_{t+k}$, available at time $t$ for the lead time $t + k$ (and with $k = 1 \dots K$), based on past observations $p_{t-1}, \dots, p_{t-n}$. For such a variable, a set of scenario $s = 1 \dots S$ is generated using the following steps:

1. generate $S$ random vectors $\mathbf{X^s}$ of dimension $K$ from a multivariate Gaussian distribution with zero mean and Pearson's covariance matrix estimated using historical observations of the target variable;

2. the final scenario $\mathbf{Y^s}$ of dimension $K$ results from the following equation:

$$Y_k^s = \hat{F}^{-1}\Big(\Phi(X_k^s)\Big) \qquad \forall k, s.$$

where $\Phi$ is the distribution function of the standard normal random variable applied to each component of $\mathbf{X^s}$, and $\hat{F}^{-1}$ is the inverse of the cumulative distribution function interpolated using the forecasted quantiles $\hat{q}_{t+k}$.

For a detailed description of the scenario generation method used in this paper, the reader may refer to the work by Pinson et al. in [27].

In this paper we use the method described to produce scenario for all the input variables of the ECT process, such as: the outdoor temperature $\hat{T}^{out}$, the heat load $\hat{Q}$, the atmospheric pressure $\hat{A}$ and the relative humidity $\hat{H}$.

## References

[1] Weather in Belgium, 2020. URL: `https://www.timeanddate.com/weather/belgium`.

[2] An, X., Si, G., Xia, T., Wang, D., Pan, E., Xi, L., 2023. An energy-efficient collaborative strategy of maintenance planning and production scheduling for serial-parallel systems under time-of-use tariffs. Applied Energy 336, 120794.

[3] Baetens, J., . Ph.D. thesis. Ghent University.

[4] Bank L., e.a., 2021. Integrating energy flexibility in production planning and control - an energy flexibility data model-based approach. Proceedings of the Conference on Production Systems and Logistics : CPSL 2021 .

[5] Bianchi, F., Bosio, B., Conte, F., Massucco, S., Mosaico, G., Natrella, G., Saviozzi, M., 2023. Modelling and optimal management of renewable energy communities using reversible solid oxide cells. Applied Energy 334, 120657.

[6] Bishop, C.M., 2006. Pattern Recognition and Machine Learning (Information Science and Statistics). Springer-Verlag, Berlin, Heidelberg.

[7] Borst, F., Strobel, N., Kohne, T., Weigold, M., 2021. Investigating the electrical demand-side management potential of industrial steam supply systems using dynamic simulation. Energies 14.

[8] Bott, A., Janke, T., Steinke, F., 2023. Deep learning-enabled mcmc for probabilistic state estimation in district heating grids. Applied Energy 336, 120837.

[9] Castro, P.M., Sun, L., Harjunkoski, I., 2013. Resource–task network formulations for industrial demand side management of a steel plant. Industrial and Engineering Chemistry Research 52, 13046–13058.

[10] Contreras-Ocaña, J.E., Ortega-Vazquez, M.A., Zhang, B., 2019. Participation of an energy storage aggregator in electricity markets. IEEE Transactions on Smart Grid 10, 1171–1183. doi:10.1109/TSG.2017.2736787.

[11] Cortinovis, G.F., Paiva, J.L., Song, T.W., Pinto, J.M., 2009. A systemic approach for optimal cooling tower operation. Energy Conversion and Management 50, 2200–2209.

[12] ELIA, 2022. Keeping the balance URL: https://www.elia.be/en/electricity-market-and-system/system-services/keeping-the-balance.

[13] ELIA, 2022. Transparency on grid data URL: www.elia.be/en/grid-data/.

[14] Engels, J., 2020. Integration of Flexibility from Battery Storage in the Electricity Market. Ph.D. thesis. URL: https://lirias.kuleuven.be/retrieve/560885.

[15] Goodfellow, I., Bengio, Y., Courville, A., 2016. Deep Learning. MIT Press. URL: http://www.deeplearningbook.org.

[16] Heffron, R., Körner, M.F., Wagner, J., Weibelzahl, M., Fridgen, G., 2020. Industrial demand-side flexibility: A key element of a just energy transition and industrial development. Applied Energy 269, 115026. doi:10.1016/j.apenergy.2020.115026.

[17] Herre, L., Tomasini, F., Paridari, K., Söder, L., Nordström, L., 2020. Simplified model of integrated paper mill for optimal bidding in energy and reserve markets. Applied Energy 279, 115857.

[18] Hosoz, M., Ertunc, H., Bulgurcu, H., 2007. Performance prediction of a cooling tower using artificial neural network. Energy Conversion and Management 48, 1349–1359.

[19] IRENA, 2022. World Energy Transitions Outlook: 1.5°C Pathway - IRENA. Technical Report.

[20] Lahariya, M., Karami, F., Develder, C., Crevecoeur, G., 2021. Physics-informed recurrent neural networks for the identification of a generic energy buffer system, in: 2021 IEEE 10th Data Driven Control and Learning Systems Conference (DDCLS), pp. 1044–1049. doi:10.1109/DDCLS52934.2021.9455657.

[21] Lombardi, M., Milano, M., 2018. Boosting combinatorial problem modeling with machine learning, AAAI Press. p. 5472–5478.

[22] Lombardi, M., Milano, M., Bartolini, A., 2017. Empirical decision model learning. Artificial Intelligence 244, 343–367. doi:10.1016/j.artint.2016.01.005.

[23] moonshotflanders, 2022. Flanders industry innovation moonshot URL: www.moonshotflanders.be/.

[24] N., F., et al., 2021. Industrial consumers' electricity market participation options: a case study of an industrial cooling process in denmark. Energy Inform 4.

[25] Pandžić, H., Dvorkin, Y., Carrión, M., 2018. Investments in merchant energy storage: Trading-off between energy and reserve markets. Applied Energy 230, 277–286. doi:10.1016/j.apenergy.2018.08.088.

[26] Papaefthymiou, G., Haesen, E., Sach, T., 2018. Power system flexibility tracker: Indicators to track flexibility progress towards high-RES systems. Renewable Energy 127, 1026–1035.

[27] Pinson, P., Madsen, H., Nielsen, H.A., Papaefthymiou, G., Klöckl, B., 2009. From probabilistic forecasts to statistical scenarios of short-term wind power production. Wind Energy 12, 51–62. doi:10.1002/we.284.

[28] Qi, X., Liu, Z., Li, D., 2008. Numerical simulation of shower cooling tower based on artificial neural network. Energy Conversion and Management 49, 724–732.

[29] Raissi, M., Perdikaris, P., Karniadakis, G., 2019. Physics-informed neural networks: A deep learning framework for solving forward and inverse problems involving nonlinear partial differential equations. Journal of Computational Physics 378, 686–707.

[30] Ramon E. Moore, R.B.K., Cloud, M.J., 2009. Introduction to Interval Analysis. MIT Press. doi:10.1137/1.9780898717716.

[31] Roald, L.A., Pozo, D., Papavasiliou, A., Molzahn, D.K., Kazempour, J., Conejo, A., 2023. Power systems optimization under uncertainty: A review of methods and applications. Electric Power Systems Research 214, 108725. doi:10.1016/j.epsr.2022.108725.

[32] Schlei-Peters, I., Kurle, D., Wichmann, M.G., Thiede, S., Herrmann, C., Spengler, T.S., 2015. Assessing combined water-energy-efficiency measures in the automotive industry. Procedia CIRP 29, 50–55.

[33] Schoepf, M., Weibelzahl, M., Nowka, L., 2018. The impact of substituting production technologies on the economic demand response potential in industrial processes. Energies 11.

[34] Schulze, C., Plank, M., Linzbach, J., Herrmann, C., Thiede, S., 2019a. Energy flexible management of industrial technical building services: a synergetic data-driven and simulation approach for cooling towers. Procedia CIRP 81, 775–780.

[35] Schulze, C., Thiede, S., Thiede, B., Kurle, D., Blume, S., Herrmann, C., 2019b. Cooling tower management in manufacturing companies: A cyber-physical system approach. Journal of Cleaner Production 211, 428–441.

[36] Shakibi, H., Shokri, A., Assareh, E., Yari, M., Lee, M., 2023. Using machine learning approaches to model and optimize a combined solar/natural gas-based power and freshwater cogeneration system. Applied Energy 333, 120607.

[37] Shoreh, M.H., Siano, P., Shafie-khah, M., Loia, V., Catalão, J.P., 2016. A survey of industrial applications of demand response. Electric Power Systems Research 141, 31–49.

[38] Starke, M.R., Kirby, B.J., Kueck, J.D., Todd, D., Caulfield, M., Helms, B., 2009. Providing reliability services through demand response: A prelimnary evaluation of the demand response capabilities of alcoa inc. URL: https://www.osti.gov/biblio/948544.

[39] Strbac, G., 2008. Demand side management: Benefits and challenges. Energy Policy 36, 4419–4426.

[40] Stull, R., 01 Nov. 2011. Wet-bulb temperature from relative humidity and air temperature. Journal of Applied Meteorology and Climatology 50, 2267 – 2269. URL: https://journals.ametsoc.org/view/journals/apme/50/11/jamc-d-11-0143.1.xml, doi:10.1175/JAMC-D-11-0143.1.

[41] Thiede, S., Kurle, D., Herrmann, C., 2017. The water–energy nexus in manufacturing systems: Framework and systematic improvement approach. CIRP Annals 66, 49–52.

[42] Vespermann, N., Delikaraoglou, S., Pinson, P., 2017. Offering strategy of a price-maker energy storage system in day-ahead and balancing markets, in: 2017 IEEE Manchester PowerTech, pp. 1–6. doi:10.1109/PTC.2017.7981050.

[43] Wang, J.G., Shieh, S.S., Jang, S.S., Wu, C.W., 2013. Discrete model-based operation of cooling tower based on statistical analysis. Energy Conversion and Management 73, 226–233.

[44] Wang, Y., Qiu, D., Sun, M., Strbac, G., Gao, Z., 2023. Secure energy management of multi-energy microgrid: A physical-

informed safe reinforcement learning approach. Applied Energy 335, 120759.

[45] Wu, J., Zhang, G., Zhang, Q., Zhou, J., Wang, Y., 2011. Artificial neural network analysis of the performance characteristics of a reversibly used cooling tower under cross flow conditions for heat pump heating system in winter. Energy and Buildings 43, 1685–1693.

[46] Xiao, K.Y.e.a., 2019. Training for faster adversarial robustness verification via inducing relu stability., in: 7th International Conference on Learning Representations, ICLR 2019.

[47] Zhang, Q., Grossmann, I.E., Heuberger, C.F., Sundaramoorthy, A., Pinto, J.M., 2015a. Air separation with cryogenic energy storage: Optimal scheduling considering electric energy and reserve markets. AIChE Journal 61, 1547–1558.

[48] Zhang, X., Hug, G., 2014. Optimal regulation provision by aluminum smelters, in: 2014 IEEE PES General Meeting — Conference Exposition, pp. 1–5.

[49] Zhang, X., Hug, G., 2015. Bidding strategy in energy and spinning reserve markets for aluminum smelters' demand response, in: 2015 IEEE Power Energy Society Innovative Smart Grid Technologies Conference (ISGT), pp. 1–5.

[50] Zhang, X., Hug, G., Kolter, Z., Harjunkoski, I., 2015b. Industrial demand response by steel plants with spinning reserve provision, in: 2015 North American Power Symposium (NAPS), pp. 1–6.

[51] Zou, P., Chen, Q., Xia, Q., He, G., Kang, C., 2016. Evaluating the contribution of energy storages to support large-scale renewable generation in joint energy and ancillary service markets. IEEE Transactions on Sustainable Energy 7, 808–818. doi:10.1109/TSTE.2015.2497283.